HHS Public Access

Author manuscript

J Am Chem Soc. Author manuscript; available in PMC 2022 November 10.

Published in final edited form as:

J Am Chem Soc. 2021 November 10; 143(44): 18617–18625. doi:10.1021/jacs.1c08551.

Decarbonylative Fluoroalkylation at Palladium(II): From Fundamental Organometallic Studies to Catalysis

Naish Lalloo, **Christian A. Malapit**, **S. Maryamdokht Taimoory**, **Conor E. Brigham**, **Melanie S. Sanford***

Department of Chemistry, University of Michigan, 930 North University Avenue, Ann Arbor, Michigan 48109, United States

Abstract

This Article describes the development of a decarbonylative Pd-catalyzed aryl–fluoroalkyl bond-forming reaction that couples fluoroalkylcarboxylic acid-derived electrophiles [$R_FC(O)X$] with aryl organometallics (Ar-M'). This reaction was optimized by interrogating the individual steps of the catalytic cycle (oxidative addition, carbonyl de-insertion, transmetalation, and reductive elimination) to identify a compatible pair of coupling partners and an appropriate Pd catalyst. These stoichiometric organometallic studies revealed several critical elements for reaction design. First, uncatalyzed background reactions between $R_FC(O)X$ and Ar–M' can be avoided by using M' = boronate ester. Second, carbonyl de-insertion and Ar–R_F reductive elimination are the two slowest steps of the catalytic cycle when $R_F = CF_3$. Both steps are dramatically accelerated upon changing to $R_F = CHF_2$. Computational studies reveal that a favorable F_2C–H----X interaction contributes to accelerating carbonyl de-insertion in this system. Finally, transmetalation is slow with X = difluoroacetate but fast with X = F. Ultimately, these studies enabled the development of an (SPhos)Pd-catalyzed decarbonylative difluoromethylation of aryl neopentylglycol boronate esters with difluoromethyl acetyl fluoride.

Graphical Abstract

*Corresponding Author: mssanfor@umich.edu.

Supporting Information

The supporting information is available free of charge at the ACS publications website.

Detailed experimental procedures, analytical data, and computational data (PDF)

X-ray crystallographic data for **II-CHF_2** (CIF)

Deposition No.: 2099725

The authors declare no competing financial interest.

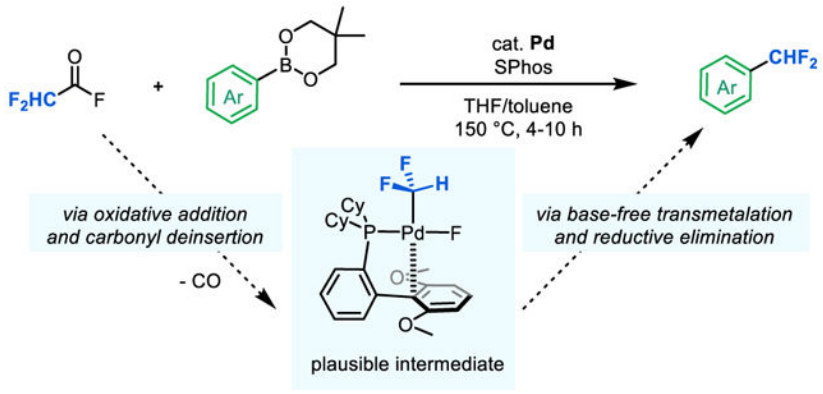

INTRODUCTION

Due to the prevalence of fluoroalkyl (R_F) substituents in bio-active molecules, there is a high demand for reagents and synthetic methods for the formation of (heteroaryl)aryl–R_F bonds.[1,2] The prevailing approach involves transition metal-catalyzed cross-coupling of aryl halide electrophiles (ArX) with fluoroalkyl nucleophiles (R_F–M).[3,4] Despite extensive work in this area, the scope and broad utility of these transformations remain limited, largely due to challenges associated with the fluoroalkyl nucleophiles.[4] The most common fluoroalkyl nucleophiles, R_3SiR_F, have limited availability for diverse R_F substituents, undergo sluggish transmetalation in the absence of bases, and exhibit poor stability in the presence of the basic additives required for transmetalation.[4,5] While some designer Ag and Zn-based fluoroalkyl nucleophiles have been developed to address these challenges, these reagents still have limitations with respect to synthetic accessibility and/or broad availability, particularly for diverse R_F groups.[4,6,7]

A complementary cross-coupling approach to form (hetero)aryl–R_F bonds would involve the reaction of fluoroalkyl carboxylic acid-derived electrophiles ($R_FC(O)X$) with (hetero)aryl nucleophiles (Ar–M', Scheme 1).[8–13] This strategy eliminates the challenges associated with transmetalation from a weakly nucleophilic R_F reagent.[4,5] Furthermore, it leverages the abundance, low cost, and stability of fluoroalkyl carboxylic acid derivatives.[13]

A putative catalytic cycle for this transformation is shown in Scheme 2 and involves (*i*) oxidative addition of $R_FC(O)X$ to form [M]–acyl complex **I**, (*ii*) carbonyl de-insertion to generate [M]–R_F intermediate **II**, (*iii*) transmetalation of the aryl nucleophile (Ar–M') to form complex **III**, and (*iv*) aryl–R_F bond-forming reductive elimination to release the product. An early study from our group established the feasibility of each of these individual steps using trifluoroacetic anhydride and diphenyl zinc as the coupling partners, and Pd[P(*o*-Tol)$_3$]$_2$/RuPhos as [M].[13a] However, catalytic turnover was not viable in this system due to a rapid uncatalyzed background reaction between the reagents to form trifluoromethyl ketones (Scheme 2, uncatalyzed acylation, *v*).

In addition to the competing background reaction, our early work identified several other limitations associated with individual steps of the catalytic cycle.[13a] For instance, direct oxidative addition of trifluoroacetic anhydride at (RuPhos)Pd^0 (step *i*) proved challenging.

As such, a two-step sequence involving initial oxidative addition at $Pd(P(o\text{-}Tol)_3)_2$ followed by a separate ligand exchange between $P(o\text{-}Tol)_3$ and RuPhos is required. Furthermore, both carbonyl de-insertion (step *ii*) and aryl–CF_3 bond-forming reductive elimination (step *iv*) were slow and/or low yielding. Finally, transmetalation (step *iii*) was limited to strongly nucleophilic organometallic reagents like diphenyl zinc.[13a]

We hypothesized that these challenges could be addressed via a mechanistic-based redesign of the catalyst and coupling partners for this reaction. In this report, we initially identify fluoroalkyl anhydrides and aryl boronate esters as compatible $R_FC(O)X$ and Ar–M' coupling partners. We then use this pair to interrogate each step of the cycle in Scheme 2 with $(SPhos)Pd^0$ as the catalyst. These stoichiometric organometallic studies provide key insights into the impact of R_F, X, and M' on each step, ultimately informing the development of a Pd-catalyzed method for the difluoromethylation of aryl boronate esters.

RESULTS AND DISCUSSION

Identifying Compatible Coupling Partners.

Our original attempts at Pd-catalyzed decarbonylative aryl fluoroalkylation were hampered by the uncatalyzed background addition of the diphenyl zinc nucleophile to the trifluoroacetic anhydride electrophile (TFAAn) to form phenyl trifluoromethyl ketone (**A**).[13a] This background reaction proceeds in 77% yield within 1 h at 25 °C (Table 1, entry 1), as determined by ^{19}F NMR spectroscopic analysis. Our initial studies focused on identifying more compatible coupling partners for the proposed catalytic transformation. We hypothesized that aryl boron reagents, which are significantly less nucleophilic than their zinc counterparts,[13a,14,22e] would minimize ketone formation. Indeed, none of the ketone **A** was formed upon stirring a $CDCl_3$ solution of trifluoroacetic anhydride (TFAAn) with phenyl boronic acid over 1 h at 25 °C. However, under these conditions a different undesired reaction, hydrolysis of the anhydride, proceeded to form trifluoroacetic acid (TFA, **B**) in quantitative yield (Table 1, entry 2). We next examined phenylboronic acid neopentylglycol ester (PhBneo) as the nucleophile, reasoning that it should minimize this hydrolysis process. Indeed, no detectable side product formation was observed upon stirring stirring a $CDCl_3$ solution of TFAAn with PhBneo over 1 or 3 h at 25 °C (Table 1, entries 3 and 4). Compatibility was also observed when using phenylboronic acid pinacol ester (PhBpin) under otherwise identical conditions (entry 5). Furthermore, compatibility with PhBneo was maintained when moving to other fluoroalkyl anhydrides (e.g., difluoroacetic anhydride) was well as other fluoroalkyl carboxylic acid derivatives (e.g., difluoroacetyl fluoride; see Supporting Information for complete details).

Catalytic Cycle: Oxidative Addition and Carbonyl De-insertion.

With a pair of compatible reagents in hand, we next focused on challenges associated with the individual steps of the catalytic cycle. As described above, previous studies with RuPhos as the ligand accessed the TFAAn oxidative addition product in two discrete steps. First, $Pd(P(o\text{-}Tol)_3)_2$, was treated with TFAAn, and this was followed by a separate ligand exchange with RuPhos.[13a] We hypothesized that replacing the large isopropoxy-substituents of RuPhos with smaller methoxy groups (of SPhos) could accelerate oxidative addition and

ligand substitution and facilitate the single-pot formation of SPhos-ligated trifluoroacetyl intermediate **I-COCF$_3$** (Figure 1). Indeed, the reaction of a THF solution of Pd[P(o-Tol)$_3$]$_2$/SPhos with TFAAn yielded **I-COCF$_3$** in 98% yield within 15 min at 25 °C (Figure 1B). Complex **I-COCF$_3$** was characterized in situ by ^{19}F and ^{31}P NMR spectroscopy, and the data are in excellent agreement with those for the reported RuPhos analogue.[13a] In particular, this complex can be clearly identified as a trifluoroacyl Pd intermediate (rather than a Pd–CF$_3$ complex) based on the diagnostic chemical shift of the CF$_3$ group (approximately −75 ppm Pd–C(O)**CF**$_3$ versus −12 ppm for Pd–**CF$_3$**).[3a,13a,14]

While Pd(P(o-Tol)$_3$)$_2$/SPhos proved highly reactive for oxidative addition of TFAAn at room temperature (Scheme 2, step *i*), carbonyl de-insertion (Scheme 2, step *ii*) at **I-COCF$_3$** remained slow in this system. After 4 h at 25 °C, no change in the ^{19}F NMR spectrum was observed, and the decarbonylated intermediate, **II-CF$_3$**, was not detected. CO de-insertion was only observed upon heating the reaction. After 30 min at 90 °C, **I-COCF$_3$** was nearly fully consumed with concomitant formation of **II-CF$_3$** in 91% yield (Figure 1C). Complex **II-CF$_3$** was characterized in situ (by analogy to the RuPhos analogue) based on its distinct broad Pd–**CF$_3$** ^{19}F NMR resonance at −11.6 ppm.[3a,13a,15,16]

We hypothesized that the rate of carbonyl de-insertion would be impacted by the nature of the migrating fluoroalkyl substituent.[17a] Thus we next explored the difluoromethyl analogue, in which a single fluorine atom is replaced by a hydrogen. This dramatically alters the size, nucleophilicity, dipole moment, and H-bond donor ability of the fluoroalkyl group,[2a–d] and all of these factors could potentially impact the carbonyl de-insertion step.[17] Furthermore, it is well-documented that Ar–CHF$_2$ bond-forming reductive elimination at Pd^{II} centers occurs under much milder conditions than analogous Ar–CF$_3$ couplings.[3,4,9a] As such, this modification should accelerate this other challenging elementary step (*iv*) of the catalytic cycle in Scheme 2.

The reaction of a THF solution of Pd[P(*o*-Tol)$_3$]$_2$/SPhos with 1 equiv of difluoroacetic anhydride (DFAAn, Figure 2A) under otherwise identical conditions afforded >99% conversion of DFAAn within 15 min at room temperature. As shown in Figure 2B, the oxidative addition product **I-COCHF$_2$** was formed in 85% yield and characterized *in situ* via ^{19}F NMR spectroscopy. This result demonstrates that oxidative addition remains fast in this system, despite the lower electrophilicity of DFAAn relative to that of TFAAn.

Interestingly, in marked contrast to the trifluoromethyl analogue, carbonyl de-insertion at **I-COCHF$_2$** also proceeded at room temperature. **II-CHF$_2$** was formed in 13% yield after 0.25 h, and the reaction was nearly complete within 10 h at 25 °C, affording **II-CHF$_2$** in 91% yield as determined by ^{19}F NMR spectroscopy (Figure 2C). Complex **II-CHF$_2$** was isolated in 61% yield and was structurally characterized by X-ray crystal-lography. An ORTEP diagram of **II-CHF$_2$**, along with representative bond distances and bond angles, are shown in Figure 3. A noteworthy feature of this structure is a short (2.38 Å) distance between H29 (from the CHF$_2$ group) and O3 (of the difluoroacetate ligand). A significantly longer distance (3.60 Å) is observed between H29 and O4. The short (2.38 Å) distance as well as the C29-H29-O3 angle of 96.9° are consistent with the existence of an attractive interaction between H29 and O3.[18]

Density functional theory (DFT) calculations[19] (M06/LANL2DZ/6–311G**) were performed to interrogate the origin of the large rate enhancement for carbonyl de-insertion at **I-COCHF$_2$** relative to **I-COCF$_3$**. This difference is counter to commonly accepted trends, where the rate is typically inversely proportional to the nucleophilicity of the migrating R group.[17a] Figure 4 shows an energy profile for 1,1-CO de-insertion at **I-COR$_F$** proceeding through **TS1-R$_F$** to initially form CO-bound complex **(CO)Pd–R$_F$**. CO dissociation then generates the experimentally observed product **II-R$_F$**. Consistent with the experimental observations, the calculations show a large (~16 kcal/mol) difference between the barrier for 1,1-de-insertion at **I-COCHF$_2$** versus **I-COCF$_3$**. In addition, the overall thermodynamics associated with conversion of **I-COCHF$_2$** to **II-CHF$_2$** + CO (DG = −18.4 kcal/mol) is significantly more favorable than for the CF_3 analogue (DG = −3.2 kcal/mol).

The computed structures show the presence of an attractive interaction with electrostatic character between H29 (of the CHF_2 group) and O3 (of the carboxylate ligand). This interaction appears to contribute significantly to both the kinetic and thermodynamic preference for carbonyl de-insertion at the CHF_2 versus CF_3 analogue[20]. In the ground state starting material, **I-COCHF$_2$**, a weak H(d+)---O(d$^-$) electrostatic contact (3.59 Å) contributes to a distortion of the coordination geometry at Pd away from square planar. For instance, the angle between the acyl and carboxylate ligands (β in Figure 4) is 97.5° in **I-COCF$_3$** (which cannot engage in this weak contact) versus 154.9° in **I-COCHF$_2$**. Given that carbonyl de-insertion transition states involve a three-coordinate metal center,[17b] this distortion makes the geometry of **I-COCHF$_2$** much closer to that of the transition state, **TS1-CHF$_2$** than in the CF_3 analogue. The H---O bond distance becomes significantly shorter moving from **I-COCHF$_2$** (3.59 Å) to **TS1-CHF$_2$** (2.69 Å) to **II-CHF$_2$** (2.37 Å). Notably, the latter closely matches that observed experimentally in the X-ray crystal structure of **II-CHF$_2$** (2.38 Å).

Further analysis of the electrostatic potential surfaces (EPSs) of **I-COCHF$_2$**, **TS1-CHF$_2$**, and **II-CHF$_2$** and of non-covalent interaction (NCI) maps of the **II-R$_F$** adducts reveal the key role of various attractive interactions (Figure 5).[20n–p] Specifically, orbital donor-acceptor interactions, electrostatic interactions, and a series of weakly attractive non-covalent bonds (dipole-induced dipole) were all observed in the -CHF_2 containing structures, most prominently in **TS1-CHF$_2$** (see Supporting Information for complete details). In contrast, the electrostatic potential surfaces of the CF_3-analogues show more diffuse dispersive repulsive interactions between the highly electronegative trifluoromethyl groups. These repulsive interactions are most pronounced in **TS1-CF$_3$**, providing further insights into the relatively high barrier to carbonyl de-insertion at **I-COCF$_3$**.

Catalytic Cycle: Transmetalation and Reductive Elimination.

We next used complex **II-CHF$_2$** to interrogate the final two steps of the catalytic cycle: transmetalation and aryl–R_F bond-forming reductive elimination (Figure 6). With boronic acid **1a** as the nucleophile, 55% conversion of **II-CHF$_2$** was observed over 0.25 h at room temperature, with concomitant formation of the difluoromethylated organic product **1** in 40% yield. None of the Pd^{II} σ-aryl intermediate **III-CHF$_2$** was detected, indicating that Ar–CHF_2 bond-forming reductive elimination is facile at room temperature.

In contrast, the boronate ester nucleophiles **1b** and **1c** showed low reactivity towards transmetalation with **II-CHF$_2$**. In both cases, >99% of **II-CHF$_2$** remained after 0.25 h at 25 °C, and only traces of **1** were detected. These results indicate that transmetalation between the Pd^{II}–difluoroacetate intermediate **II-CHF$_2$** and aryl boronate esters is likely to be a key bottleneck in catalysis.

We hypothesized that this issue could be addressed by changing the X-type ligand on Pd^{II} from trifluoroacetate to a more reactive fluoride.[21,22] Previous work[23,24] has demonstrated that transition metal fluoride complexes exhibit high transmetalation activity towards various aryl boron nucleophiles. To generate a Pd^{II}–F intermediate, we treated a THF solution of **II-CHF$_2$** with anhydrous tetramethylammonium fluoride (Me_4NF) for 0.5 h at 25 °C (Figure 7). This resulted in complete consumption of **II-CHF$_2$** and the appearance of a broad ^{19}F NMR resonance at −349.5 ppm, which is diagnostic for a metal-fluo-ride.[21] While this intermediate could not be isolated cleanly, the addition of boronate ester **1b** resulted in consumption of the Pd–F signal within 15 min at 25 °C and formation of the reductive elimination product **1** in 27% yield (Figure 7). Again, the putative intermediate **III-CHF$_2$** was not detected. Overall, this sequence demonstrates that a fluoride ligand enables the targeted transmetalation/reductive elimination sequence with **1b**, thus closing the formal catalytic cycle in this system.

Development of Catalytic Reaction.

The organometallic studies described above demonstrate that each individual step of the catalytic cycle in Scheme 2 can proceed at room temperature. As such, our initial catalysis attempts focused on the room temperature SPhos/Pd[P(o-Tol)$_3$]$_2$-catalyzed decarbonylative coupling of DFAAn with boronate ester **1b** in the presence of metal fluoride (MF) sources. As summarized in Figure 8, none of these reactions (with Me_4NF, Bu_4NF, or CsF) yielded the target difluoromethylated product **1**. However, in the crude ^{19}F NMR spectra of reactions that used CsF as the fluoride source, difluoroacetyl fluoride (DFAF) observed as a major byproduct.

We noted that acid fluorides are significantly less electrophilic than their anhydride counterparts[8j], which could result in slower oxidative addition. To address this potential issue, we next explored elevated temperatures. Gratifyingly, at 130 °C using excess CsF relative to DFAAn, the coupling product **1** was observed, albeit in modest (22%) yield (Figure 8). The stoichiometric studies suggest that at 130 °C carbonyl de-insertion should also be feasible for the $-CF_3$ and $-CF_2CF_3$ analogues. As such, we explored the analogous catalytic reactions using TFAAn and pentafluoropropionic anhydride (PFPAn) at 130 °C. As shown in Figure 8, 4-trifluoromethylbenzonitrile and 4-pentafluoroethylbenzonitrile were formed in these transformations, in modest yields of 5% and 4%, respectively. In all three decarbonylative fluoroalkylation reactions a significant amount of the corresponding fluoroalkyl acid was observed in the crude mixture, consistent with competing decomposition of the anhydrides with traces of water in the fluoride salts.

Moving forward, we focused on optimizing catalytic decarbonylative difluoromethylation, since this was the highest yielding reaction among those in Figure 8. To eliminate the need

for the hygroscopic fluoride additives, we independently synthesized anhydrous DFAF as a concentrated solution in THF (see SI for full details) and deployed it directly as the electrophile for cross-coupling.[23,24] As shown in Table 2, entry 1, none of product **1** was detected at room temperature with DFAF as the electrophile, consistent with slow oxidative addition. However, upon heating this reaction to 130 °C, **1** was formed in 51% yield (entry 3). The reaction was further optimized with respect to reagent stoichiometry, temperature, solvent, and reaction time.[25] Under the optimized conditions (10 mol % $Pd[P(o\text{-}Tol)_3]_2$, 20 mol % of SPhos, 5 equiv of DFAF, and 1 equiv of **1b** in a mixture of THF:toluene at 150 °C for 5 h), **1** was formed in 92–93% yield as determined by ^{19}F NMR spectroscopic analysis and was isolated in 77% yield (see SI for details).

We next evaluated the scope of arene nucleophiles for this transformation. As summarized in Table 3, a variety of neopentylglycol boronate esters bearing electron withdrawing substituents (**1–13**) reacted to afford modest to excellent yields of difluoromethylarene products.[26] Nitriles (**1, 2**), ketones (**3–5**), esters (**6–8**), sulfoxides (**11**), sulfonamides (**12, 13**) were well-tolerated under the reaction conditions. In addition, azole derivatives (**9, 10**) reacted in low to modest yields. Boronate esters bearing fluorinated substituents also underwent difluoromethylation in good to excellent yields but proved too volatile for isolation (see SI). Interestingly, boronate ester derivatives bearing electron donating substituents, such as methyl, phenyl, or benzyl ethers, showed low reactivity[27] under these conditions (typically <5% yield). ^{19}F NMR spectroscopic analysis of these low yielding reactions showed significant quantities of unreacted DFAF and no identifiable organic by-products. Ongoing efforts are focused on interrogating the mechanistic origin of this limitation and developing second generation catalysts to overcome it.

CONCLUSIONS

In summary, this Article presents a detailed investigation of decarbonylative cross-couplings between fluoroalkyl carboxylic acid-derived electrophiles and aryl boron nucleophiles. The combination of stoichiometric organometallic and computational studies unveiled several key findings that ultimately enabled the development of a catalytic difluoromethylation reaction. First, unusually low barriers are observed for the key carbonyl de-insertion step at $(SPhos)Pd^{II}(C(O)CHF_2)(X)$ complexes relative to their trifluoromethyl analogues. Several attractive non-covalent interactions involving the acidic CHF_2 hydrogen appear to play a crucial role in lowering this barrier, a finding that could prove more broadly useful in the future development of decarbonylative couplings with these electrophiles.

The generation of a Pd–fluoride intermediate proved critical for promoting the challenging transmetalation step of the sequence. This finding led to the use of difluoroacetyl fluoride as the electrophile in catalysis to directly access a ‘transmetalation-active’ Pd-fluoride intermediate in situ and enable base-free transmetalation. While similar effects have been observed at nickel centers, this report is rare example of base-free cross-coupling of an acid fluoride derivative at Pd.[24i] Overall, we expect this study to engender interest in the unique properties of fluoroalkyl groups and the reactivity of metal–fluoroalkyl complexes in the context of catalytic reaction development.

Supplementary Material

Refer to Web version on PubMed Central for supplementary material.

ACKNOWLEDGMENT

We acknowledge Dr. Jeff Kampf for X-ray crystallographic analysis of compound **II-CHF_2**. This work was supported by the NIH NIGMS (R35GM1361332). We also acknowledge computational resources and services provided by Compute Canada (SHARCNET: www.sharcnet.ca) and the Jaguar program supported by Dr. John F. Trant's group facility at the University of Windsor.

ABBREVIATIONS

THF	Tetrahydrofuran
DCM	dichloromethane
Et_2O	diethyl ether
DFAF	difluoroacetyl fluoride
DFAAn	difluoroacetic anhydride
TFAAn	trifluoroacetic anhydride
DFA	difluoroacetic acid
TFA	trifluoroacetic acid
PFPAn	pentafluoropropionic anhydride
PFPA	pentafluoropropionic acid
TMAF	tetramethyl ammonium fluoride
TBAF	tetrabutylammonium fluoride
RT	room temperature
SPhos	2-dicylcohexylphosphino-2',6'-dimethoxybiphenyl

REFERENCES

(1). On fluorine in molecules:(a)Müller K; Faeh C; Diederich F Fluorine in pharmaceuticals: looking beyond intuition. Science 2007, 317, 1881–1886. [PubMed: 17901324] (b)Purser S; Moore PR; Swallow S; Gouverneur V Fluorine in medicinal chemistry. Chem. Soc. Rev 2008, 37, 320–330. [PubMed: 18197348] (c)Hagmann WK The many roles for fluorine in medicinal chemistry. J. Med. Chem 2008, 51, 4359–4369. [PubMed: 18570365] (d)Wang J; Sanchez-Roselló M; Aceña JL; del Pozo C; Sorochinsky AE; Fustero S; Soloshonok VA; Liu H Fluorine in pharmaceutical industry: fluorine-containing drugs introduced to the market in the last decade (2001−2011). Chem. Rev 2014, 114, 2432–2506. [PubMed: 24299176] (e)Liang T; Neumann CN; Ritter T Introduction of fluorine and fluorine-containing functional groups. Angew. Chem., Int. Ed 2013, 52, 8214–8264.(f)Caron S Where does fluorine come from? A review on the challenges associated with the synthesis of organofluorine compounds. Org. Process Res. Dev 2020, 24, 470–480.(g)Shah P; Westwell AD; The role of fluorine in medicinal chemistry. J. Enzyme Inhib. Med. Chem 2007, 22, 527–540. [PubMed: 18035820] (h)O'Hagan D Fluorine in health care:

organofluorine containing blockbuster drugs. J. Fluor. Chem 2010, 131, 1071–1081.(i)Jackel C; Salwiczek M Koksch B Fluorine in native protein environment - how the spatial demand and polarity of fluoroalkyl groups affect protein folding. Angew. Chem. Int. Ed 2006, 45, 4198–4203.

(2). On the properties and synthesis of difluoromethylarenes:(a)Zafrani Y; Yeffet D; Sod-Moriah G; Berliner A; Amir D; Marciano D; Gershonov E; Saphier S Difluoromethyl ioisostere: examining the “lipophilic hydrogen bond donor” concept. J. Med. Chem 2017, 60, 797–804. [PubMed: 28051859] (b)Zafrani Y; Saphier S; Gershonov E Utilizing the CF_2H moiety as a H-bond-donated group in drug discovery. Future Med. Chem 2020, 12, 361–365. [PubMed: 32027173] (c)Erickson JA; McLoughlin JI Hydrogen bond donor properties of the difluoromethyl group. J. Org. Chem 1995, 60, 1626–1631.(d)Sessler CD; Rahm M; Becker S; Goldberg JM; Wang F; Lippard SJ CHF_2, a hydrogen bond donor. J. Am. Chem. Soc 2017, 139, 9325–9332. [PubMed: 28576078] (e)Rageot D; Beaufils F; Borsari C; Dall’Asen A; Neuberger M; Hebeisen P; Wymann MP Scalable, economical, and practical synthesis of 4-(difluoromethyl)pyridine-2-amine, a fey intermediate for lipid kinase inhibitors. Org. Process Res. Dev 2019, 23, 2416–2424.

(3). Metal-catalyzed nucleophilic trifluoromethylation via cross-coupling:(a)Cho EJ; Senecal TD; Kinzel T; Zhang Y; Watson DA; Buchwald SL The palladium-catalyzed trifluoromethylation of aryl chlorides. Science 2010, 328, 1679–1681. [PubMed: 20576888] (b)Morimoto H; Tsubogo T; Litvinas ND; Hartwig JF A broadly applicable copper reagent for trifluoromethylations and perfluoroalkylations of aryl iodides and bromides. Angew. Chem., Int. Ed 2011, 50, 3793–3798.

(4). Metal-catalyzed nucleophilic fluoroalkylation:(a)Fier PS; Hartwig JF Copper-mediated difluoromethylation of aryl and vinyl iodides. J. Am. Chem. Soc 2012, 134, 5524–5527. [PubMed: 22397683] (b)Jiang X-L; Chen Z-H; Xu X-H; Qing F-L Copper-mediated difluoromethylation of electron-poor aryl iodides at room temperature. Org. Chem. Front 2014, 1, 774–776.(c)Prakash GKS; Ganesh SK; Jones J-P; Kulkarni A; Masood K; Swabeck JK; Olah GA Copper-mediated difluoromethylation of (hetero)aryl iodides and β-styryl halides with tributyl(difluoromethyl)stannane. Angew. Chem., Int. Ed 2012, 51, 12090–12094.(d)Gu Y, Leng X & Shen Q Cooperative dual palladium/silver catalyst for direct difluoromethylation of aryl bromides and iodides. Nat Commun. 2014, 5, 1–7.(e)Chang D; Gu Y; Shen Q Pd-Catalyzed difluoromethylation of vinyl bromides, triflates, tosylates, and nonaflates. Chem. Eur. J 2015, 21, 6074–6078. [PubMed: 25752832] (f)Nakamura Y; Fujiu M; Murase T; Itoh Y; Serizawa H; Aikawa K; Mikami K Cu-catalyzed trifluoromethylation of aryl iodides with trifluoromethylzinc reagent prepared in situ from trifluoromethyl iodide. Beilstein J. Org. Chem 2013, 9, 2404–2409. [PubMed: 24367406] (g)Aikawa K; Nakamura Y; Yokota Y; Toya W; Mikami K Stable but reactive perfluoroalkylzinc reagents: application in ligand-free copper-catalyzed perfluoroalkylation of aryl iodides. Chem. Eur. J 2015, 21, 96–100. [PubMed: 25393887] (h)Aikawa K; Toya W; Nakamura Y; Mikami K Development of (trifluoromethyl)zinc reagent as trifluoromethyl anion and difluorocarbene sources. Org. Lett 2015, 17, 4996–4999. [PubMed: 26430875] (i)Xu L; Vicic DA; Direct difluoromethylation of aryl halides via base metal catalysis at room temperature. J. Am. Chem. Soc 2016, 138, 2536–2539. [PubMed: 26883690] (j)Serizawa H; Ishii K; Aikawa K; Mikami K Copper-Catalyzed difluoromethylation of aryl iodides with (difluoromethyl)zinc reagent. Org. Lett 2016, 18, 3686–3689. [PubMed: 27442584]

(5). Furuya T; Kamlet AS Catalysis for fluorination and trifluoromethylation. Nature 2011, 473, 470–477. [PubMed: 21614074]

(6). On the reagent $TMSCF_3$:(a)Liu X; Wang M Liu Q. Trifluoromethyltrimethylsilane: nucleophilic trifluoromethylation and beyond. Chem. Rev 2015, 115, 683–730. [PubMed: 24754488] (b)Krishnamoorthy S; Kothandaraman J; Saldana J; Surya Prakash GK Direct difluoromethylation of carbonyl compounds by using $TMSCF_3$: the right conditions. Eur. J. Chem 2016, 4965–4969.(c)Xie Q; Li L; Zhu Z; Zhang R; Ni C; Hu J From C_1 to C_2: $TMSCF_3$ as a precursor to pentafluoroethylation. Angew. Chem. Int. Ed 2018, 57, 13211–13215. (d)Johnston CP; West TH; Dooley RE; Reid M; Jones AB; King EJ; Leach AG Lloyd-Jones GC Anion-initiated trifluoromethylation by $TMSCF_3$: deconvolution of the siliconate-carbonanion dichotomy by stopped-flow NMR/IR. J. Am. Chem. Soc 2018, 140, 11112–11124. [PubMed: 30080973]

(7). Mudarra AL; Martinez de Salinas S; Perez-Temprano MH Beyond the traditional roles of Ag in catalysis: the transmetalating ability of organosilver(i) species in Pd-catalysed reactions. Org. Biomol. Chem 2019, 17, 1655–1667. [PubMed: 30474675]

(8). For reviews on carboxylic acids and their derivatives as electrophiles in cross-coupling:(a)Baudoin O New approaches for decarboxylative biaryl coupling. Angew. Chem. Int. Ed 2007, 46, 1373–1375.(b)Gooßen K, Rodriguez N, Gooßen LJ, Carboxylic acids as substrates in homogenous catalysis. Angew. Chem. Int. Ed 2008, 47, 3100–3120.(c)Yu DG.; B. J. Li.; Z. J. Shi. Exploration of new C−O electrophiles in cross-coupling reactions. Acc. Chem. Res 2010, 43, 1486–1495; [PubMed: 20849101] (d)Rodriguez N, Gooßen LJ, Decarboxylative coupling reactions: a modern strategy for C–C-bond formation. Chem. Soc. Rev 2011, 10, 5030–5048;(e)Cornella J, Larrosa I, Decarboxylative carbon-carbon bond-forming transformations of (hetero)aromatic carboxylic acids. Synthesis 2012, 44, 653–6.(f)Hoover JM Mechanistic aspects of copper-catalyzed decarboxylative coupling reactions of (hetero)aryl carboxylic acids. Comment. Inorg. Chem 2017, 37, 169–200.(g)Takise R; Muto K; Yamaguchi J Cross-coupling of aromatic esters and amides. Chem. Soc. Rev 2017, 46, 5864–5888. [PubMed: 28685781] (h)Guo L; Rueping M Decarbonylative cross-couplings: Nickel catalyzed functional group interconversion strategies for the construction of complex organic molecules. Acc. Chem. Res 2018, 51, 1185–1195. [PubMed: 29652129] (i)Meng G; Szostak M *N*-Acyl-glutarimides: Privileged scaffolds in amide N–C bond cross-coupling. Eur. J. Org. Chem 2018, 2352–2365.(j)Zhao Q; Szostak M Redox-neutral decarbonylative cross-couplings coming of age. ChemSusChem 2019, 12, 2983–2987. [PubMed: 30908875] (k)Blanchard N; Bizet V Acid fluorides in transition-metal catalysis: a good balance between stability and reactivity. Angew. Chem. Int. Ed 2019, 58, 6814–6187.(l)Ogiwara Y; Sakai N Acyl fluorides in late transition-metal catalysis. Angew. Chem. Int. Ed 2020, 59, 574–594. (m)Wang Z; Wang X; Nishihara Y Nickel or palladium-catalyzed decarbonylative tranformations of carboxylic acid derivatives. Chem Asian J. 2020, 15, 1234–1247. [PubMed: 32125073] (n)Zheng Y-L; Newman SG Cross-coupling reactions with esters, aldehydes, and alcohols. Chem. Commun 2021, 57, 2591–2604.(o)Fahandej-Sadi A; Lundgren RJ Copper-mediated synthesis of monofluoro aryl acetates via decarboxylative cross-coupling. Synlett 2017, 28, 2886–2890. (p)Moon PJ; Yin S; Lundgren RJ Ambient decarboxylative arylation of malonate half-esters via oxidative catalysis. J. Am. Chem. Soc 2016, 138, 13826–13829. [PubMed: 27736064]

(9). For relevant difluoromethylation examples:(a)Pan F; Boursalian GB; Ritter T Palladium-catalyzed decarbonylative difluoromethylation of acid chlorides at room temperature. Angew. Chem. Int. Ed 2018, 57, 16871–16876.(b)Feng Z, Min Q, Fu X, An L, Zhang X Chlorodifluoromethane-triggered formation of difluoromethylated arenes catalysed by palladium. Nat. Chem 2017, 9, 918–923. [PubMed: 28837166] (c)Hori K, Motohashi H, Saito D, Mikami K Precatalyst effects of Pd-catalyzed cross-coupling difluoromethylation of aryl boronic acids. ACS Catal. 2019, 9, 417–421.

(10). Fluorinated carboxylic acids in decarboxylative coupling:(a)Beatty JW; Douglas JJ; Cole KP; Stephenson CRJ A Scalable and operationally simple radical trifluoromethylation. Nat. Commun 2015, 6, 7919–7925. [PubMed: 26258541] (b)Kyohide M; Etsuko T; Midori A; Kiyosi K A convenient trifluoromethylation of aromatic halides with sodium trifluoroacetate. Chem. Lett 1981, 10, 1719–1720.(c)Chen M; Buchwald SL Rapid and efficient trifluoromethylation of aromatic and heteroaromatic compounds using potassium trifluoroacetate enabled by a flow system. Angew. Chem. Int. Ed 2013, 52, 11628–11631.(d)Ambler BR; Zhu L; Altman RA Copper-catalyzed synthesis of trifluoroethylarenes from benzylic bromodifluoroacetates. J. Org. Chem 2015, 80, 8449–8457. [PubMed: 26225803] (e)Ambler BR; Santosh P; Altman RA Ligand-controlled regioselective copper-catalyzed trifluoromethylation to generate (trifluoromethyl)allenes. Org. Lett 2015, 17, 2506–2509. [PubMed: 25910053] (f)Carr GE; Chambers RD; Holmes TF; Parker DG Sodium perfluoroalkane carboxylates as sources of perfluoroalkyl groups. J. Chem. Soc., Perkin Trans 1988, 1, 921–926.(g)Johansen MB; Lindhardt AT Copper-catalyzed and additive free decarboxylative trifluoromethylation of aromatic and heteroaromatic iodides. Org. Biomol. Chem 2020, 18, 1417–1425. [PubMed: 32016267] (h)Zapf A; Beller M Fine chemical synthesis with homogeneous palladium catalysts: examples, status, and trends. Topics in Catalysis. 2002, 19, 101–109.

(11). (a)Sun AC; McClain EJ; Beatty JW; Stephenson CRJ Visible light-mediated decarboxylative alkylation of pharmaceutically relevant heterocycles. Org. Lett 2018, 20, 3487–3490. [PubMed: 29856641] (b)Tung TT; Christensen SB; Nielsen J Diflluoroacetic acid as a new reagent for direct C–H difluoromethylation of heteroaromatic compounds. Chem. Eur. J 2017, 23, 18125–18128. [PubMed: 28945302]

(12). For other examples of fluoroalkyl carboxylic acid derivatives being used as a fluoroalkyl sources, see:(a)Yang M-H; Orsi DL; Altman RA Ligand-controlled regiodivergent palladium-catalyzed decarboxylative allylation reaction to access α, α-difluoroketones. Angew. Chem. Int. Ed 2015, 54, 2361–2365.(b)Yang M-H; Hunt JR; Sharifi N; Altman RA Palladium catalysis enables benzylation of α, α-difluoroketone enolates. Angew. Chem. Int. Ed 2016, 55, 9080–9083.(c)Ambler BR; Yang M-H; Altman RA Metal-catalyzed decarboxylative fluoroalkylation reactions. Synlett 2016, 27, 2747–2755. [PubMed: 28260839]

(13). Fluorinated carboxylic acids in decarbonylative coupling:(a)Maleckis A; Sanford MS Catalytic cycle for palladium-catalyzed decarbonylative trifluoromethylation using trilfuoroacetic esters as the CF_3 source. Organometallics 2014, 33, 2653–2660;(b)Brigham CE; Malapit CA; Lalloo N; Sanford MS Nickel-catalyzed decarbonylative synthesis of fluoroalkyl thioethers. ACS Catal. 2020, 10, 8315–8320. [PubMed: 34306801]

(14). Bakhmutov VI; Bozoglian F; Gomez K; Gonzalez G; Grushin VV; Macgregor SA; Martin E; Miloserdov FM; Novikov MA; Panitier JA; Romashov LV CF_3–Ph reductive elimination from [(XantPhos}Pd(CF_3)(Ph)]. Organometallics 2012, 31, 1315–1328.

(15). Lennox AJJ; Lloyd-Jones GC Selection of boron reagents for Suzuki–Miyaura coupling. Chem. Soc. Rev 2014, 43, 412–443. [PubMed: 24091429]

(16). We conducted an analogous stoichiometric oxidative addition and carbonyl de-insertion experiment with pentafluoropropionic anhydride (PFPAn, $R_F = -CF_2CF_3$). As summarized in Figures S9 and S10, the reaction with PPAn proceeded nearly identically to that with TFAAn, showing fast oxidative addition but very slow carbonyl de-insertion at room temperature [<1% yield of the carbonyl de-insertion product after 4 h at room temperature].

(17). For relative rates in carbonylation reactions, see:(a)Shusterman AJ; Tamir I; Pross A The mechanism of organometallic migration reactions. A configuration mixing approach. J. Organomet. Chem 1988, 340, 203–222.(b)Ortuno MA; Busra D; Cramer CJ Mechanism of Pd-catalyzed decarbonylation of biomass-derived hydrocinnamic acid to styrene following activation as an anhydride. Inorg. Chem 2016, 55, 4124–4131 [PubMed: 27077600]

(18). (a)Johnston RC; Cheong HY C-H---O non-classical hydrogen bonding in the stereomechanics of organic transformations: theory ad recognition. Org. Biomol. Chem 2013, 11, 5057–5064. [PubMed: 23824256] (b)Gilli P; Pretto L; Bertolasi V; Gilli GPredicting hydrogen-bond strengths from acid-base molecular properties. The pK_a slide rule: toward the solution of a long-lasting problem. Acc. Chem. Res 2009, 42, 33–44. [PubMed: 18921985]

(19). For DFT methods, see:(a)Schrödinger Release 2019–2: Macro-Model, Schrödinger, LLC, New York, NY, 2019.b)Schrödinger Release 2019–2: Maestro, Schrödinger, LLC, New York, NY, 2019.(b)Frisch MJ; Trucks GW; Schlegel HB; Scuseria GE; Robb MA; Cheeseman JR; Scalmani G; Barone V; Mennucci B; Petersson GA; Nakatsuji H; Caricato M; Li X; Hratchian HP; Izmaylov AF; Bloino J; Zhang G; Sonnenberg JL; Hada M; Ehara M; Toyota K; Fukuda R; Hasegawa J; Ishida M; Nakajima T; Honda Y; Kitao O; Nakai H; Vreven T; Montgomery JA; Peralta JE Jr.; Ogliaro F; Bearpark M; Heyd JJ; Brothers E; Kudin KN; Staroverov VN; Kobayashi R; Normand J; Raghavachari K; Rendell A; Burant JC; Iyengar SS; Tomasi J; Cossi M; Rega N; Millam JM; Klene M; Knox JE; Cross JB; Bakken V; Adamo C; Jaramillo J; Gomperts R; Stratmann RE; Yazyev O; Austin AJ; Cammi AR; Pomelli C; Ochterski JW; Martin RL; Morokuma K; Zakrzewski VG; Voth GA; Salvador P; Dannenberg JJ; Dapprich S; Daniels AD; Farkas Ö; Foresman JB; Ortiz JV; Cioslowski J; Fox DJ Gaussian 09, Revision C.02; Gaussian, Inc.: Wallingford, CT, 2009.(c)Roy LE; Hay PJ; Martin RL Revised Basis Sets for the LANL Effective Core Potentials. J. Chem. Theory Comput 2008, 4, 1029–1031. [PubMed: 26636355] (d)Zhao Y, Truhlar DG. Density Functionals with Broad Applicability in Chemistry. Acc. Chem. Res 2008, 41, 157–167. [PubMed: 18186612] (e)Huzinaga S, Gaussian Basis Sets for Molecular Calculations, Elsevier Science Pub. Co., Amsterdam, 1984. 15 P. J. Hay and W. R. Wadt, J. Chem. Phys, 1985, 82, 299–310.(f)Hay PJ and Wadt WR, Ab initio effective core potentials for molecular calculations. Potentials for the transition metal atoms Sc to Hg. J. Chem. Phys 1985, 82, 270–283.(g)Gonzalez C; Schlegel HB An improved algorithm for reaction path following. J. Chem. Phys, 1989, 90, 2154–2161;(h)Gonzelez C; Schlegel HB Reaction Path Following in Mass-Weighted Internal Coordinates. J. Phys. Chem, 1990, 94, 5523–5527.(i)Barone V; Cossi M Quantum Calculation of Molecular Energies and Energy Gradients in Solution by a Conductor Solvent Model. J. Phys. Chem. A, 1998, 102, 1995–2001;(j)Cossi

M; Rega N; Scalmani G; Barone VJ Energies, structures, and electronic properties of molecules in solution with the C-PCM solvation model. Comput. Chem, 2003, 24, 669–681.(k)Reed AE; Weinstock RB; Weinhold F Natural population analysis. J. Chem. Phys, 1985, 83, 735–746; (l)Reed AE; Weinhold F Natural localized molecular orbitals. J. Chem. Phys, 1985, 83, 1736–1740;(m)Reed AE; Curtiss LA; Weinhold F Intermolecular interactions from a natural bond orbital, donor-acceptor viewpoint. Chem. Rev, 1988, 88, 899–926.(n)Glendening ED; Reed AE; Carpenter JE; Weinhold F NBO Version 3.1;(o)Contreras-García J; Johnson ER; Keinan S; Chaudret R; Piquemal J-P; Beratan DN; Yang W NCIPLOT: A program for plotting noncovalent regions. J. Chem. Theory Comput 2011, 7, 625–632. [PubMed: 21516178] (p)Shakourian-Fard M; Kamath G; Jamshidi Z Trends in physisorption of ionic liquids on boron-nitride sheets. J. Phys. Chem. C 2014, 118, 26003–26016.

(20). Trifluoroacetic anhydride (TFAAn) and pentafluoropropionic anhydride (PFPAn) both undergo rapid oxidative addition at room temperature but require elevated temperatures for carbonyl de-insertion. Both TFAAn and PFPAn lack the acidic hydrogen found in DFAAn and require high temperatures for carbonyl de-insertion. See the Supporting Information (p. S8–13) for more details.

(21). (a)Fraser SL, Antipin M. Yu., Khroustalyov VN, Grushin VV, Molecular fluoro palladium complexes J. Am. Chem. Soc 1997, 119, 4769–4770.(b)Beweries T; Brammer L; Jasim NA; McGrady JE; Perutz RN, Whitwood AC Energetics of halogen bonding of group 10 metal fluoride complexes. J. Am. Chem. Soc 2011, 133, 14338–14348. [PubMed: 21851113]

(22). For recent example of studies on transmetalation-active organometallic complexes with organoboron and silicon, see:(a)Carrow BP; Hartwig JF Distinguishing between pathways for transmetalation in Suzuki-Miyaura reactions. J. Am. Chem. Soc 2011, 133, 2116–2119. [PubMed: 21280669] (b)Amatore C, Jutand A & Le Duc G The triple role of fluoride ions in palladium-catalyzed Suzuki–Miyaura reactions: unprecedented transmetalation from [$ArPdFL_2$] complexes. Angew. Chem. Int. Ed 2012, 51, 1379–1382.(c)Thomas AA & Denmark SE Pre-transmetalation intermediates in the Suzuki–Miyaura reaction revealed: the missing link. Science 2016, 352, 329–332. [PubMed: 27081068] (d)Malapit CA; Bour JR; Brigham CE; Sanford MS Base-free nickel-catalysed decarbonylative Suzuki-Miyaura coupling of acid fluorides. Nature 2018, 563, 100–104. [PubMed: 30356210] (e)Malapit CA; Bour JR; Laursen SR; Sanford MS Mechanism and scope of nickel-catalyzed decarbonylative borylation of carboxylic acid fluorides. J. Am. Chem. Soc 2019, 141, 17322–17330. [PubMed: 31617708] (f)Malapit CA; Borrell M; Milbauer MW; Brigham CE; Sanford MS Nickel-catalyzed decarbonylative amination of carboxylic acid esters. J. Am. Chem. Soc 2020, 142, 5918–5923. [PubMed: 32207616]

(23). For reviews on utility of acid fluorides in decarbonylative cross-coupling, see refs 8k–m.

(24). For examples of utility of acid fluorides in decarbonylative cross-coupling, see refs 20d, 20f, and:(a)Keaveney ST; Schoenebeck F Palladium-catalyzed decarbonylative trifluoromethylation of acid fluorides. Angew. Chem. Int. Ed 2018, 57, 4073–4077.(b)Wang Z; Wang X; Nishihara Y Nickel-catalysed decarbonylative borylation of aroyl fluorides. Chem. Commun 2018, 54, 13969–13972.(c)Ogiwara Y; Sakurai Y; Hattori H; Sakai N Palladium-catalyzed reductive conversion of acyl fluorides via ligand-controlled decarbonylation. Org. Lett 2018, 20, 4204–4208. [PubMed: 29963866] (d)Okuda Y; Xu J; Ishida T; Wang C.-a.; Nishihara Y Nickel-catalyzed decarbonylative alkylation of aroyl fluorides assisted by Lewis-acidic organoboranes. ACS Omega 2018, 3, 13129–13140. [PubMed: 31458033] (e)Sakurai S; Yoshida T; Tobisu M Iridium-catalyzed decarbonylative coupling of acyl fluorides with arenes and heteroarenes via C-H activation. Chem. Lett 2019, 48, 94–97.(f)Ogiwara Y; Iino Y; Sakai N Catalytic C–H/C–F coupling of azoles and acyl fluorides. Chem. Eur. J 2019, 25, 6513–6516. [PubMed: 30941769] (g)Wang X; Wang Z; Liu L; Asanuma Y; Nishihara Y Nickel-catalyzed decarbonylative stannylation of acyl fluorides under ligand-free conditions. Molecules 2019, 24, 1671–1682. (h)Wang X; Wang Z; Nishihara Y Nickel/copper-cocatalyzed decarbonylative silylation of acyl fluorides. Chem. Commun 2019, 55, 10507–10510.(i)Kayumov M; Zhao J-N; Mirzaakhmedov S; Wang D-Y; Zhang A Synthesis of arylstannanes via palladium-catalyzed decarbonylative coupling of aroyl fluorides. Adv. Synth. Catal 2020, 362, 776–781.(j)Chen Q; Fu L; Nishihara Y Palladium/copper-cocatalyzed decarbonylative alkynylation of acyl fluorides with alkynylsilanes: synthesis of unsymmetrical diarylethynes. Chem. Commun 2020, 56, 7977–7980.(k)Wang Z; Wang X; Ura Y; Nishihara Y Nickel-catalyzed decarbonylative cyanation of acyl chlorides.

Org. Lett 2019, 21, 6779–6784. [PubMed: 31389711] (l)Sakurai Y; Oqiwara Y; Sakai N Palladium-catalyzed annulation of acyl fluorides with norbornene via decarbonylation and CO reinsertion. Chem. Eur. J 2020, 26, 12972–12977. [PubMed: 32452619] (m)He B; Liu X; Li H; Zhang X; Ren Y; Su W Rh-Catalyzed general method for directed C–H functionalization via decarbonylation of in-situ-generated acid fluorides from carboxylic acids. Org. Lett 2021, 23, 4191–4196. [PubMed: 33979175]

(25). Optimal yields are obtained by conducting this reaction in tall, 10-mL scintillation vials, and other vessels examined resulted in in significantly diminished yields. We hypothesize that having additional head space for the reaction is beneficial due to the gaseous nature of DFAF and THF under the reaction conditions. See p. S34 for complete details about the selection of reaction vessel.

(26). The mass balance in the catalytic reaction was evaluated via ^{19}F NMR spectroscopy using 2-(4-fluorophenyl)-5,5-dimethyl-1,3,2-dioxaborinane as the substrate. After 3 h, 17% of the difluoromethylated product [1-(difluoromethyl)-4-fluorobenzene], 14% of the protodeboronation product [fluorobenzene], and 43% of the aryl boron starting material were observed, accounting for 74% of the mass balance. Neither 4-fluorophenylboronic acid nor 4,4’-difluorobiphenyl were detected. See p. S32–33 for additional details.

(27). Given the poor reactivity of electron-rich aryl boronate nucleophiles in the catalytic reaction, we evaluated the fluoride-mediated transmetalation of **II-CHF$_2$** with the p-OCH_3 substituted substrate **19b**. The difluoromethylated product **19** was formed in 26% yield (nearly identical to the 27% yield of **1** in Figure 7), suggesting that the transmetalation step is not the origin of the poor reactivity of electron-rich boronate esters in the catalytic reaction. See the Supporting Information (pages S18–19) for additional details.

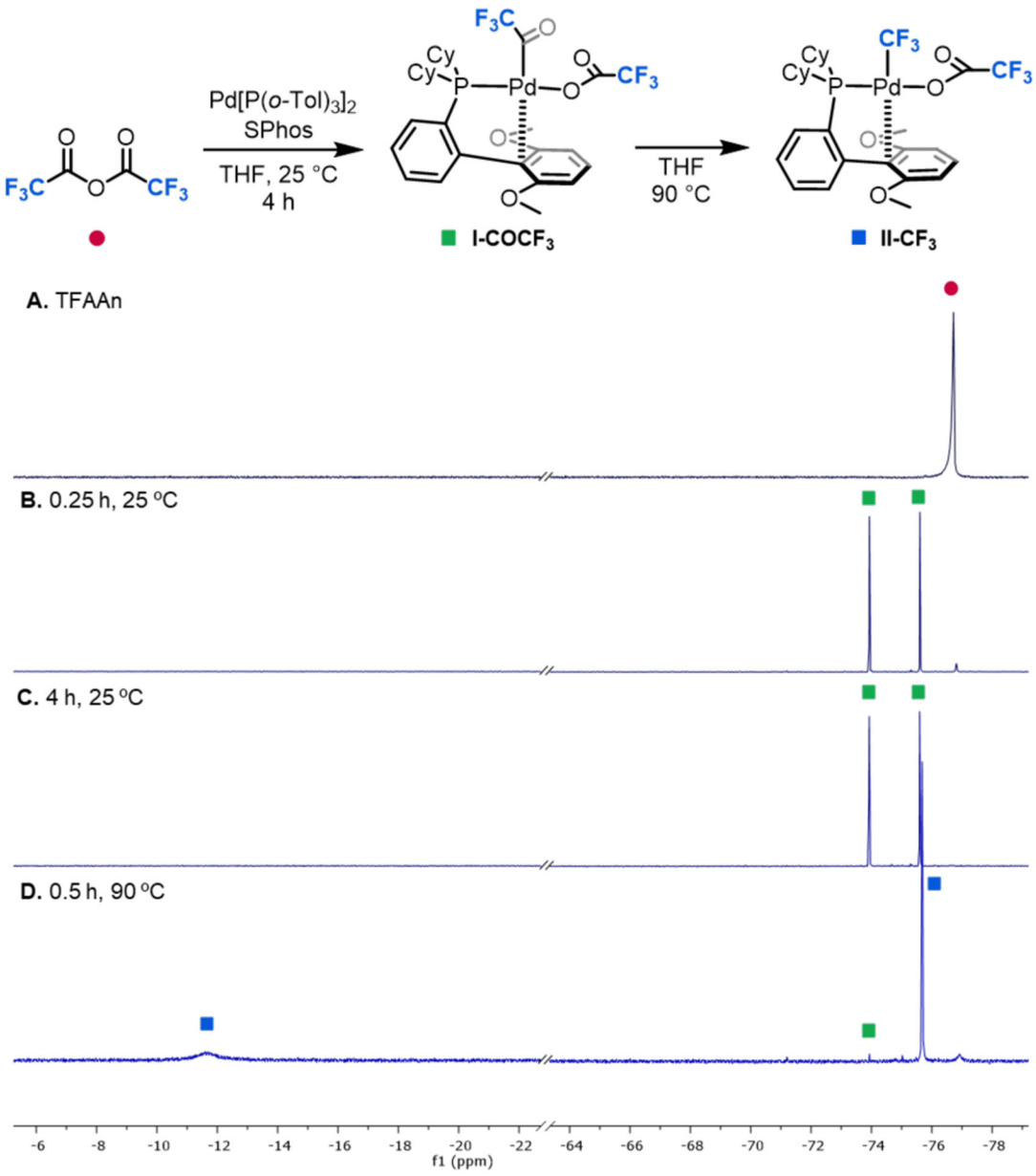

Figure 1.

Oxidative addition and carbonyl de-insertion of TFAAn at SPhos/Pd^0 in THF. ^{19}F NMR spectra of (A) TFAAn; (B) Reaction of TFAAn with SPhos/Pd^0 in THF after 0.25 h at room temperature; (C) Reaction of TFAAn with SPhos/Pd^0 in THF after 4 h at room temperature; (D) Reaction heated to 90°C for 0.5 h. Spectra are referenced to 4-fluorotoluene (−119.85 ppm).

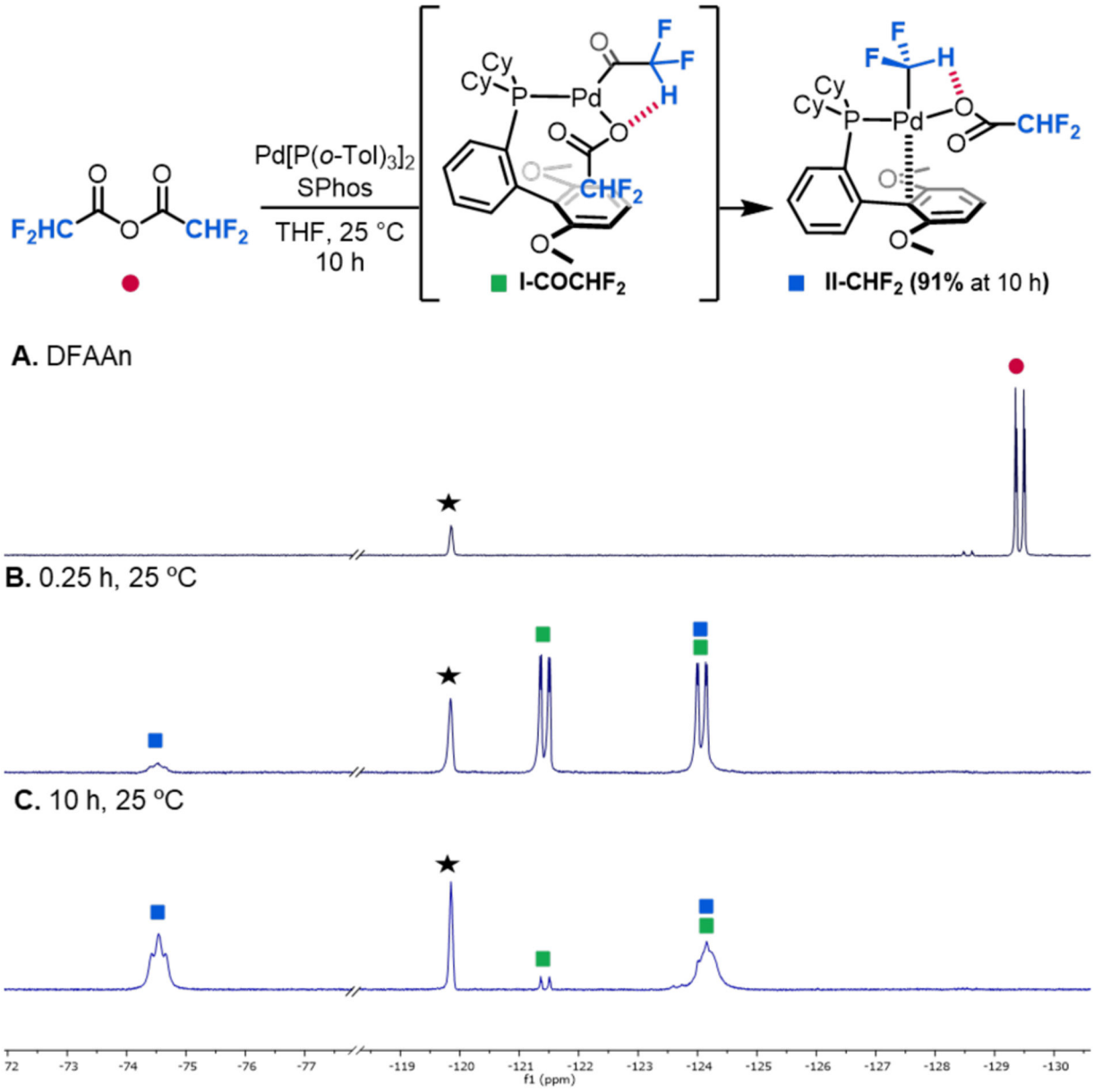

Figure 2.

Oxidative addition and carbonyl de-insertion of DFAAn at SPhos/Pd^0 in THF. ^{19}F NMR spectrum of (A) DFAAn; (B) Reaction of DFAAn with SPhos/Pd^0 in THF after 15 min at room temperature; (C) Reaction of DFAAn with SPhos/Pd^0 in THF after 10 h at room temperature. Black star represents 4-fluorotoluene (−119.85 ppm, internal standard).

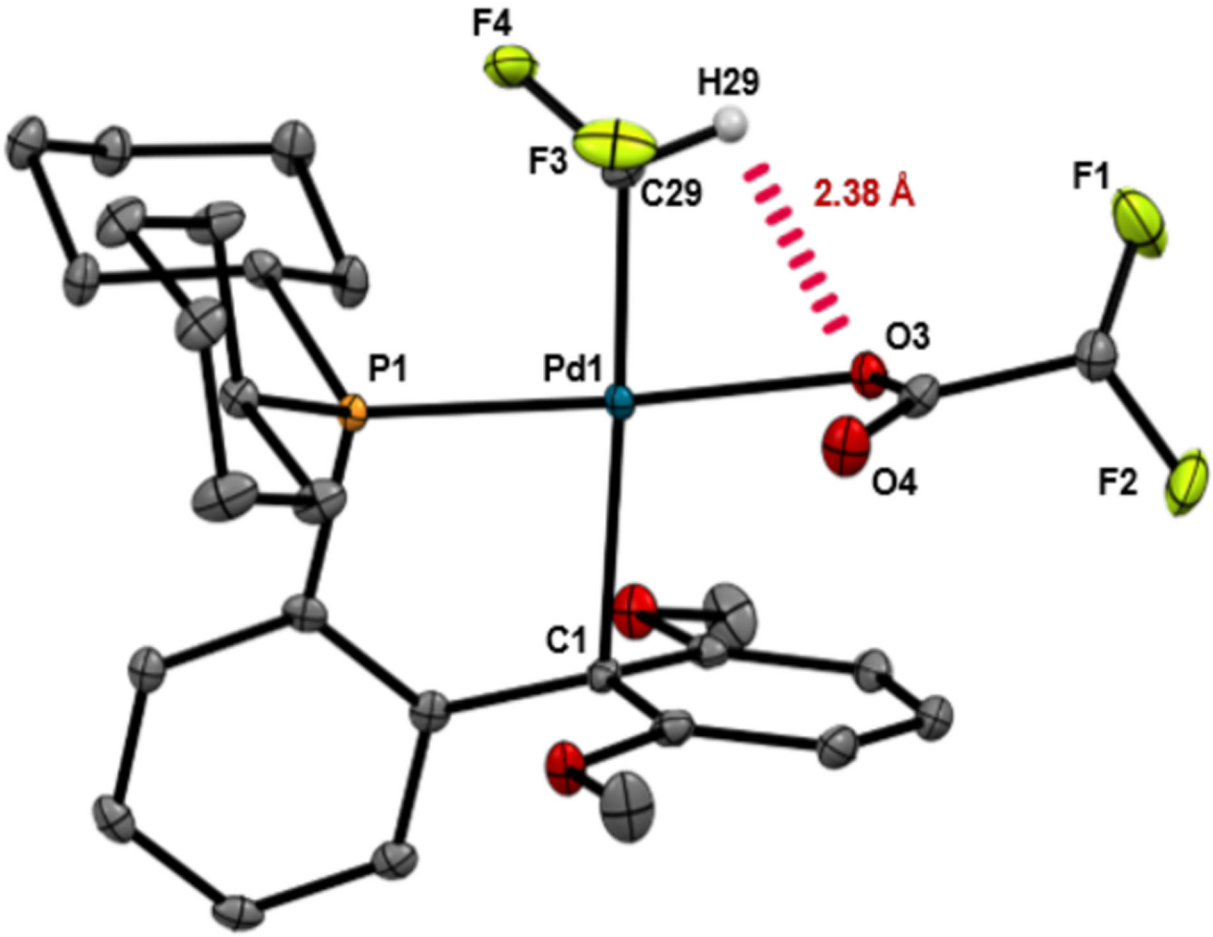

Figure 3.

ORTEP diagram of **II-CHF$_2$**. Select hydrogen atoms are omitted for clarity. Selected bond lengths (Å) and angle (deg): O3–Pd1 2.11, O4–Pd1 3.09, C29–Pd1 1.99, C1–Pd1 2.46; H29---O3 2.38, H29---O4 3.60; C29–Pd1–O3 81.7, C29–H29---O3 96.9.

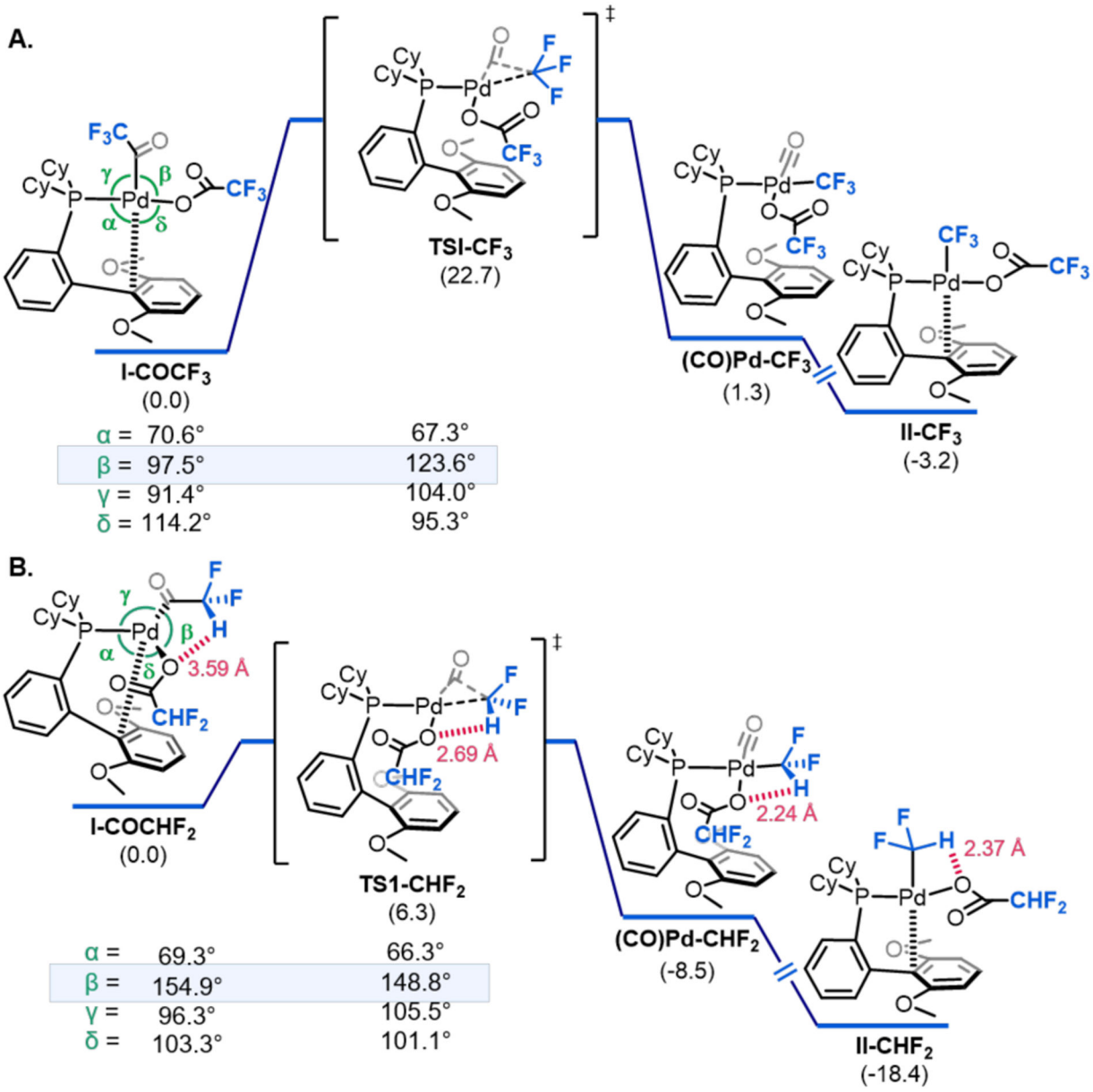

Figure 4.

Energetics (the preferred binding mode highlighted as conformer A, see SI for details) for the carbonyl de-insertion process at (A) **I-COCF$_3$** and (B) **I-COCHF$_2$** with selected key angles α, β, γ, and δ for **I-COR$_F$** and **TS1-R$_F$**.

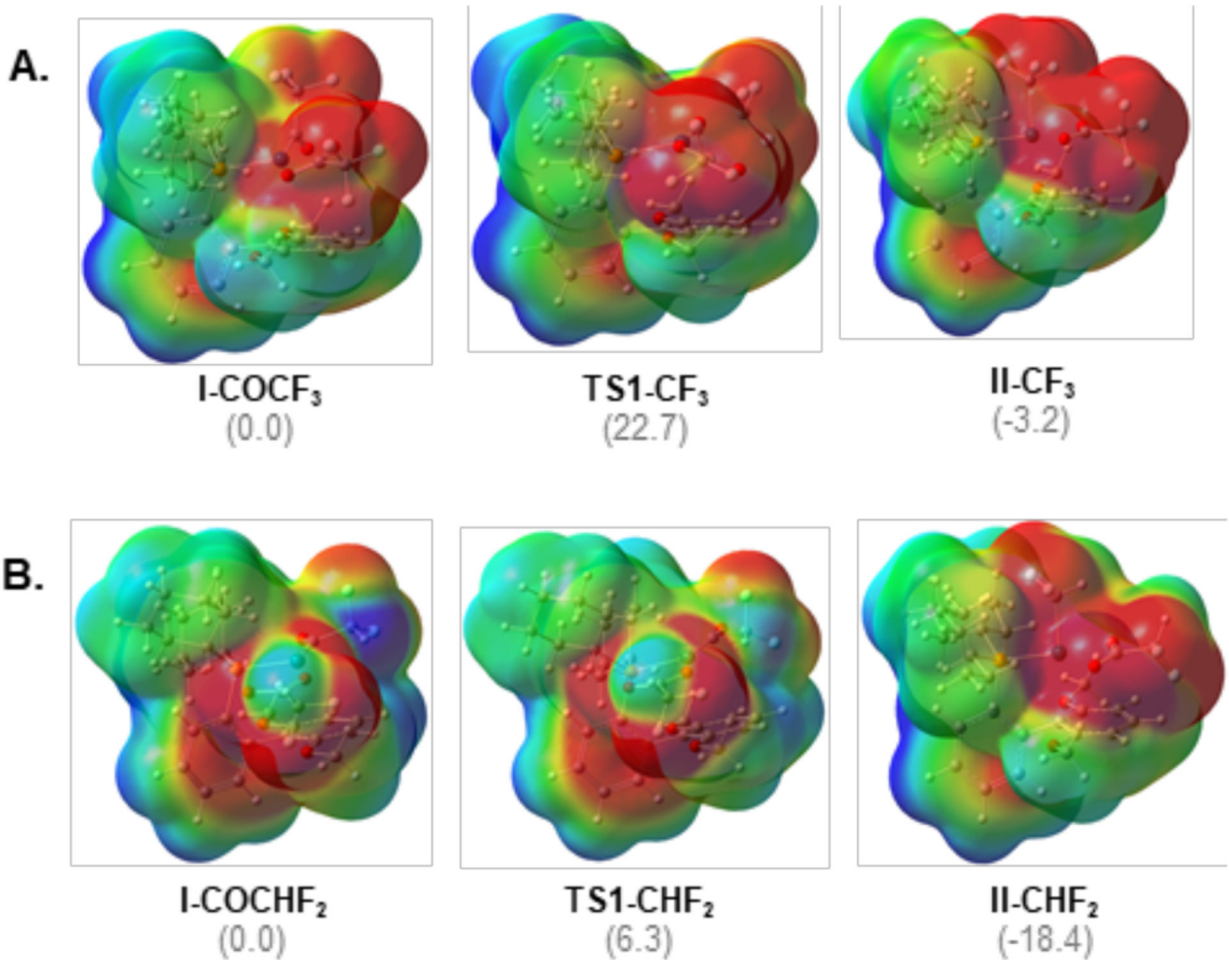

Figure 5.

Electrostatic potential surfaces (for the optimal conformer A, see SI for details) generated for (A) **I-COCF$_3$**, **TS1-CF$_3$**, and **II-CF$_3$**; (B) **I-COCHF$_2$**, **TS1-CHF$_2$**, and **II-CHF$_2$**. Energies are in represented in kcal/mol.

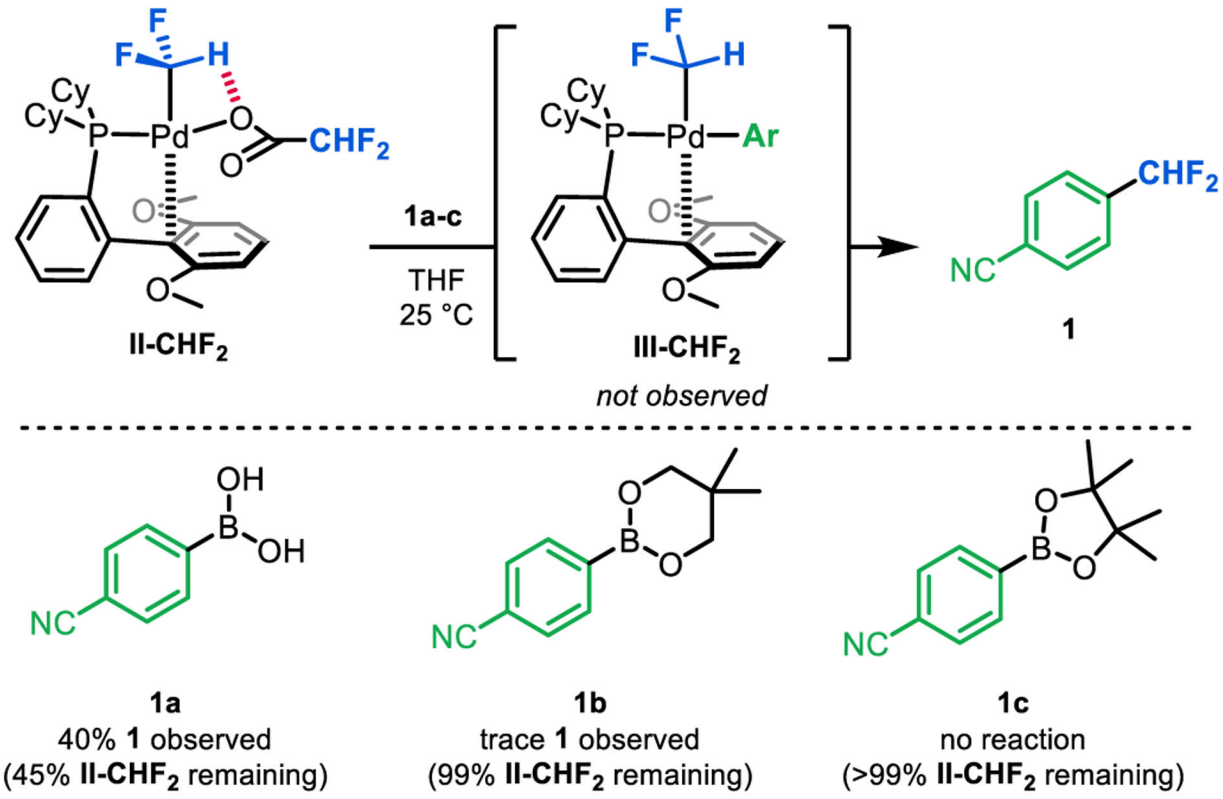

Figure 6.

Transmetalation/reductive elimination sequence between **II-CHF$_2$** and aryl boron nucleophiles **1a-c**.

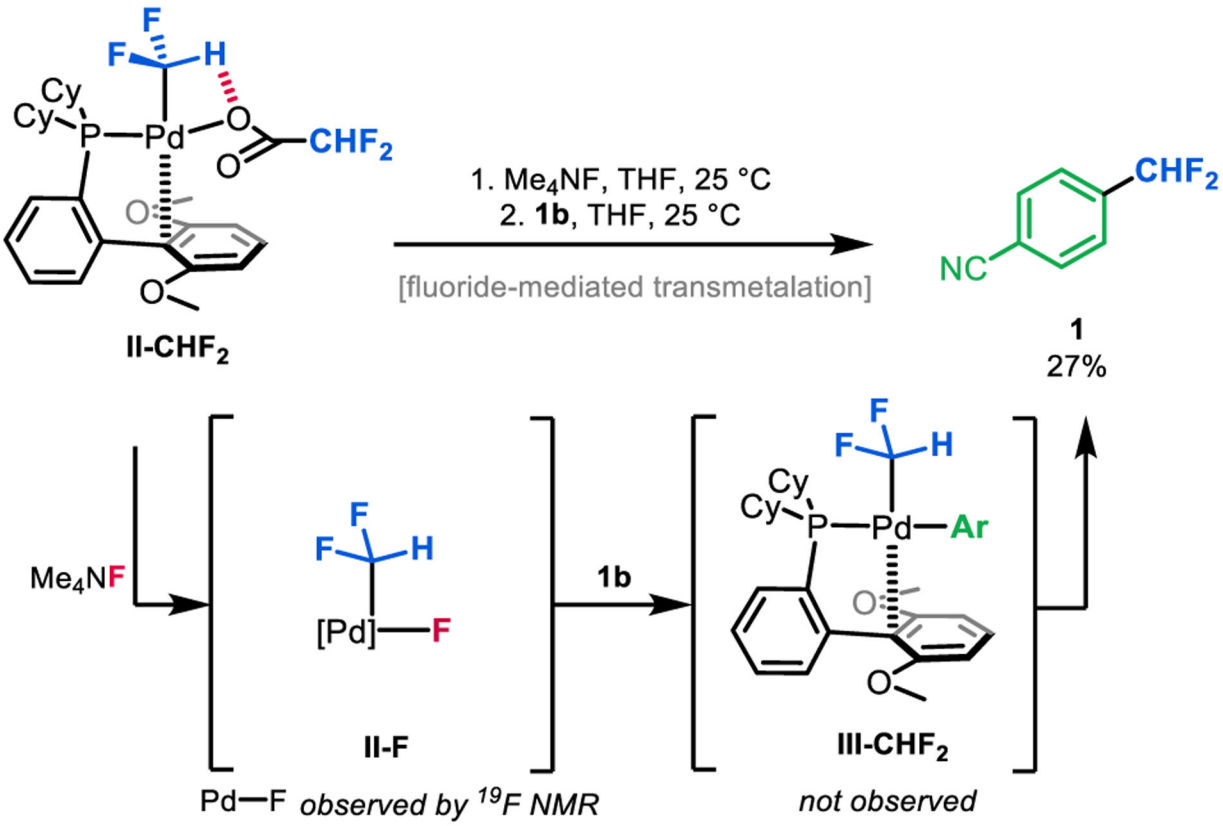

Figure 7.

Generation of a Pd–F intermediate facilitates transmetalation with organoboron reagent **1b** and subsequent reductive elimination (steps *iii* and *iv* in Scheme 2).

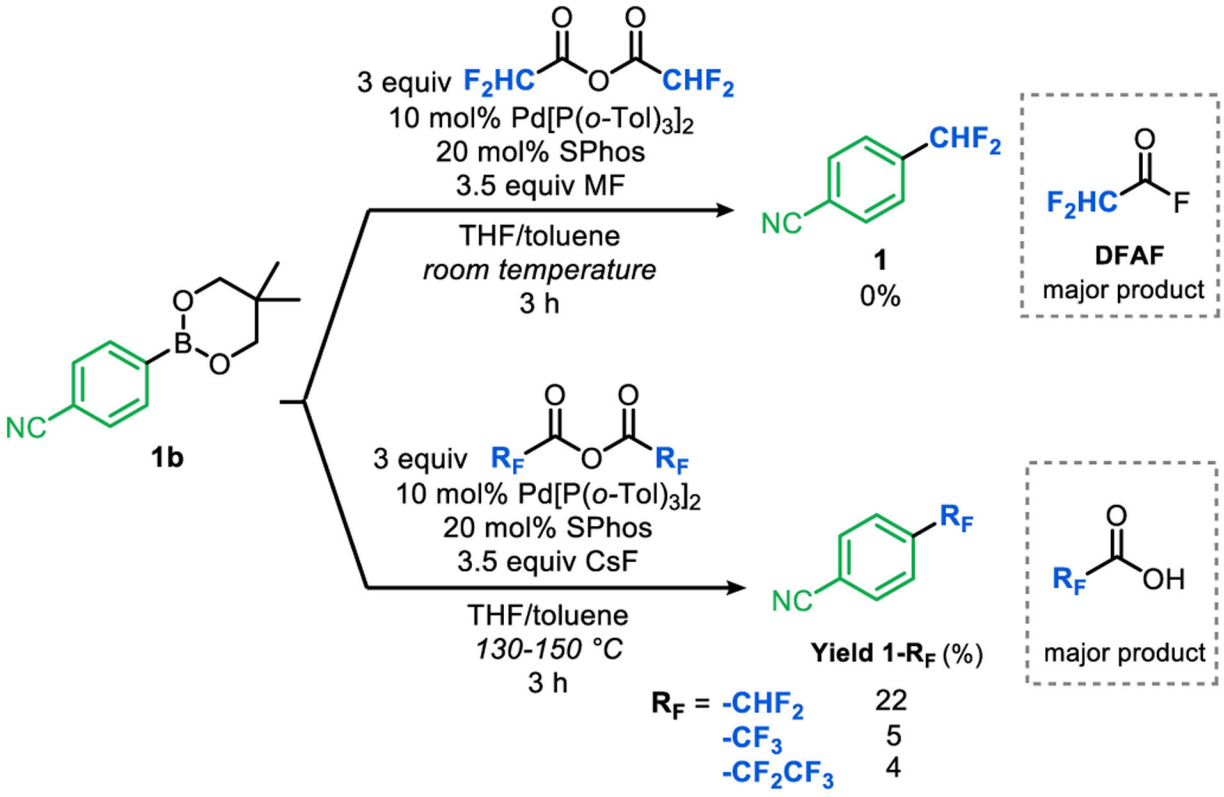

Figure 8.
Initial attempts at catalysis using DFAAn and fluoride salts.

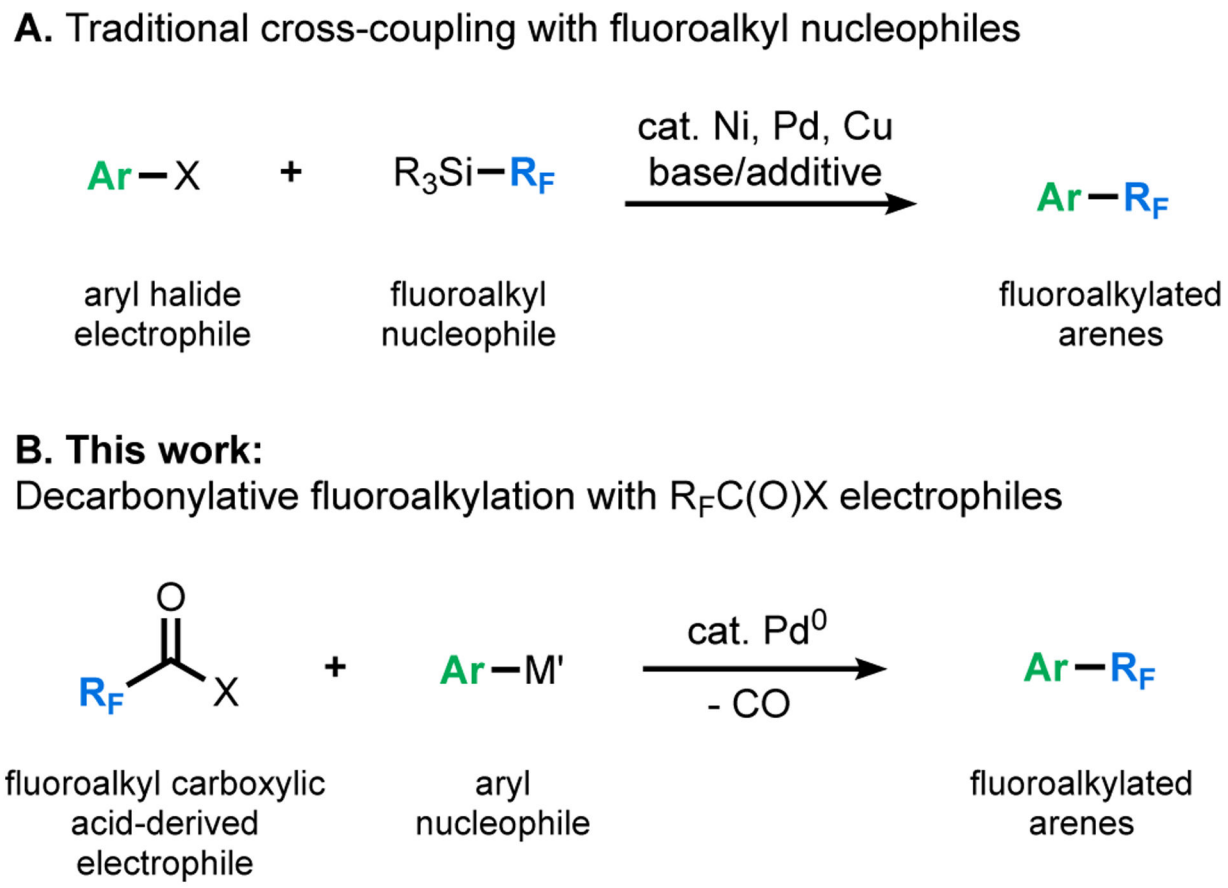

Scheme 1.

(A) Traditional fluoroalkylative cross-coupling using fluoroalkyl nucleophiles; (B) **This work**: decarbonylative fluoroalkylation with fluoroalkyl carboxylic acid-derived electrophiles.

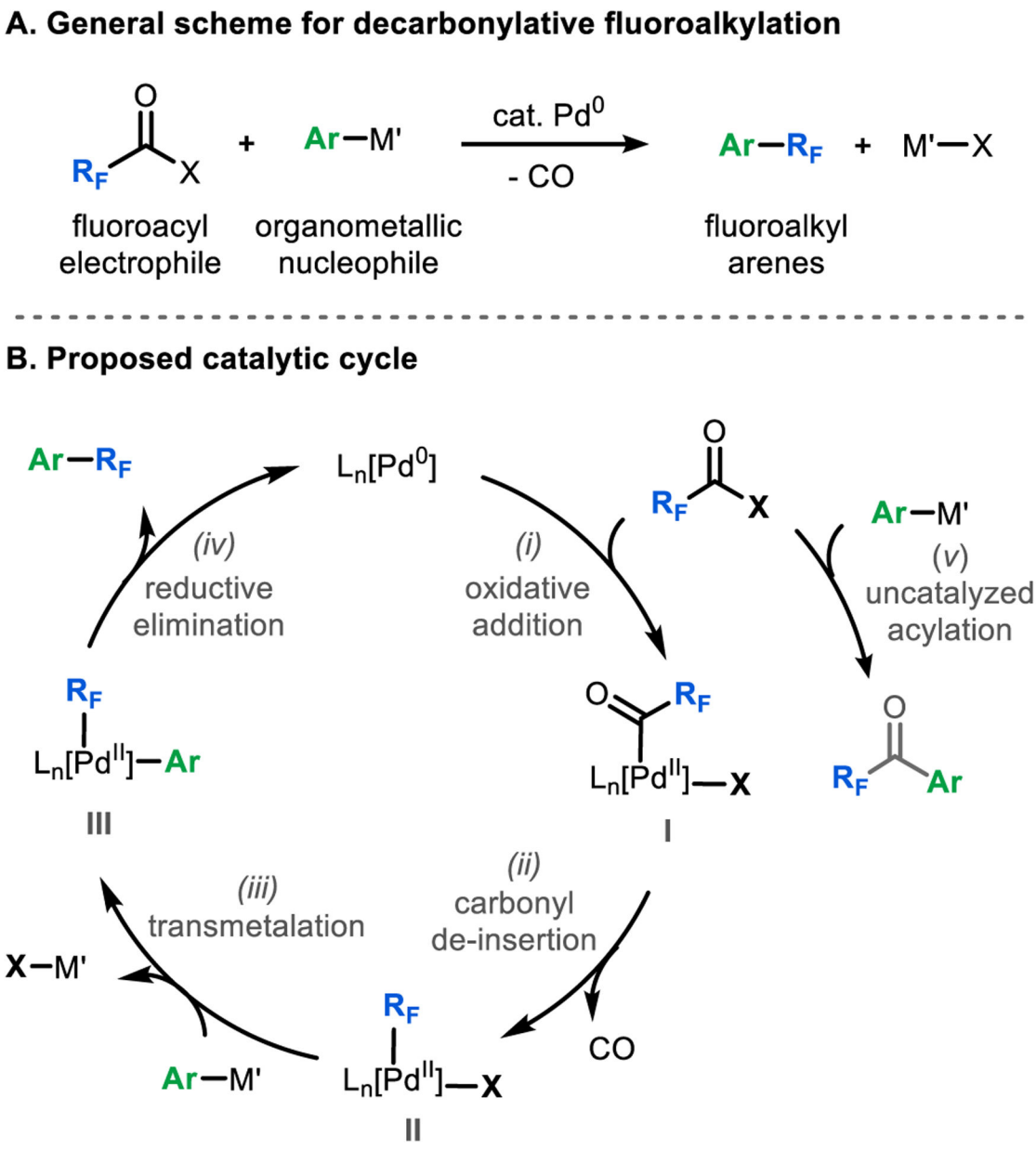

Scheme 2.

(A) General reaction scheme for decarbonylative fluoroalkylation and (B) proposed catalytic cycle with undesired acylation shown.

Table 1.

Compatibility of TFAAn with different aryl nucleophiles.

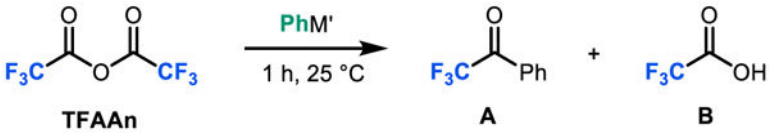

entry	PhM'	yield A	yield B
1	Ph_2Zn	77%	0%
2	$PhB(OH)_2$	<1%	>95%
3	PhBneo	<1%	<1%
4[a]	PhBneo	<1%	<1%
5	PhBpin	<1%	<1%

[a]25 °C for 3 h.

Table 2.

Optimization of difluoromethylation of **1a** with DFAF.

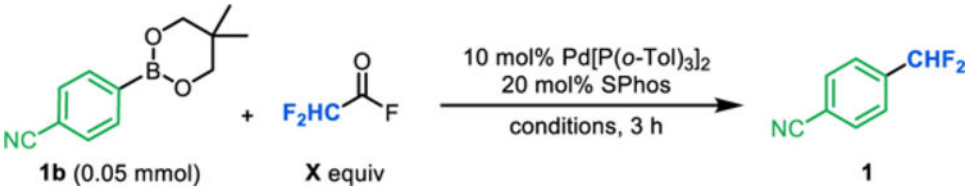

entry	X	T (°C)	solvent	yield (%)[a]
1	1	25	THF	<1
2	1	100	THF	29
3	1	130	THF:toluene (1:1)	51
4	3	130	THF:toluene (1:1)	58
5	5	130	THF:toluene (1:1)	67
6	5	150	THF:toluene (1:1)	86
7	5	150	THF:dioxane (1:1)	72
8[b]	5	150	THF:toluene (1:1)	93
9[b]	5	150	THF:toluene (1:2)	92

[a]Yields determined by ^{19}F NMR with 4-fluorotoluene internal standard.

[b]Reaction was run for 5 h.

Table 3.

Scope of aryl boronate esters for the catalytic electrophilic decarbonylative difluoromethylation using difluoroacetyl fluoride.

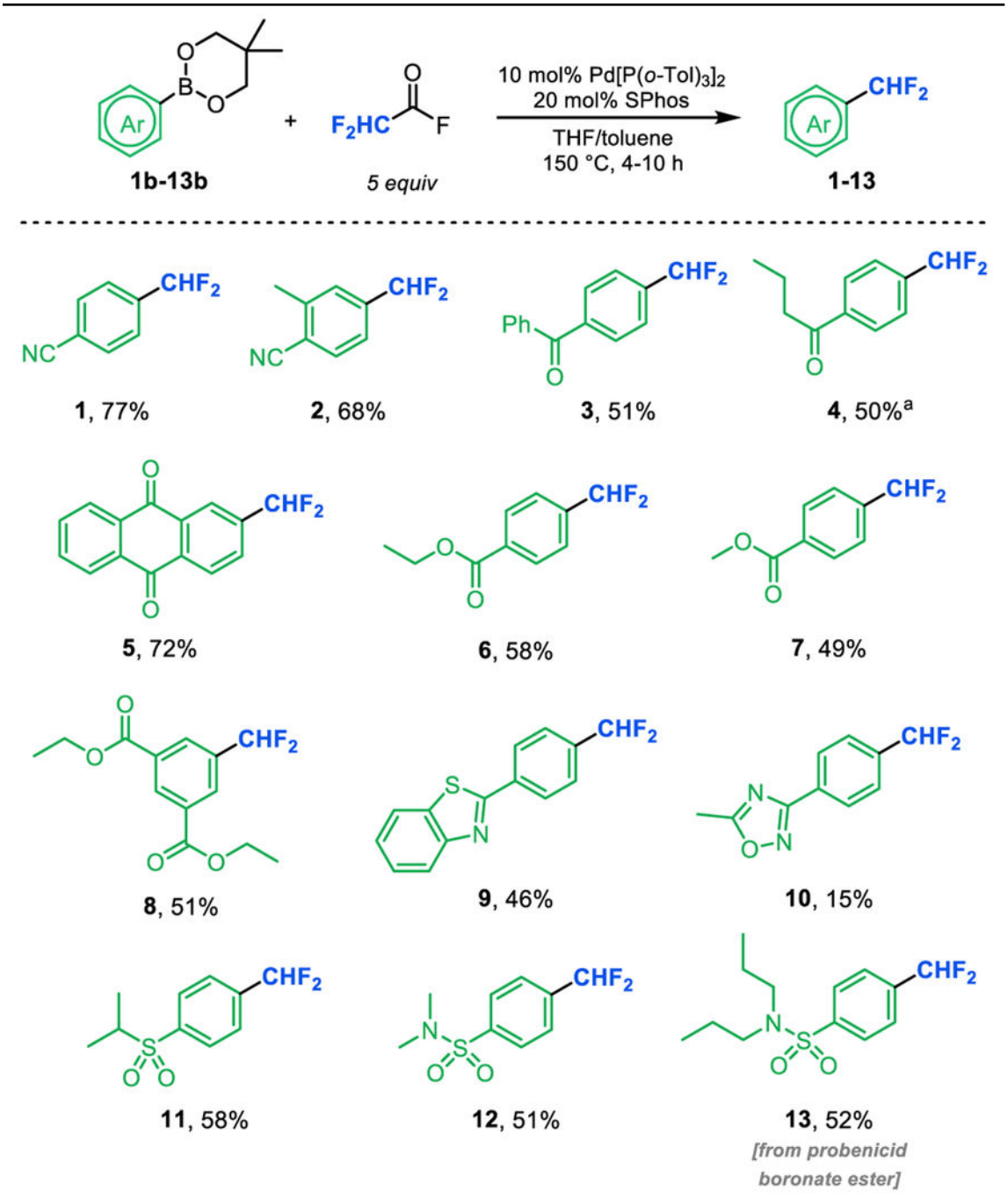

[a]15 mol% Pd[P(*o*-tol)3]2/30 mol% SPhos used for catalysis. See Supporting Information for details.